# Acoustomagnonic Spin Hall Effect in Honeycomb Antiferromagnets

Ryotaro Sano,[1,*] Yuya Ominato,[2,3] and Mamoru Matsuo[2,4,5,6]
[1]Department of Physics, Kyoto University, Kyoto 606-8502, Japan
[2]Kavli Institute for Theoretical Sciences, University of Chinese Academy of Sciences, Beijing 100190, China
[3]Waseda Institute for Advanced Study, Waseda University, Shinjuku, Tokyo 169-8050, Japan
[4]CAS Center for Excellence in Topological Quantum Computation, University of Chinese Academy of Sciences, Beijing 100190, China
[5]RIKEN Center for Emergent Matter Science (CEMS), Wako, Saitama 351-0198, Japan
[6]Advanced Science Research Center, Japan Atomic Energy Agency, Tokai 319-1195, Japan

(Received 19 June 2023; accepted 3 May 2024; published 5 June 2024)

The recently discovered Van der Waals antiferromagnets have suffered from the lack of a comprehensive method to study their magnetic properties. Here, we propose an ac intrinsic magnon spin Hall current driven by surface acoustic waves as a novel probe for such antiferromagnets. Our results pave the way towards mechanical detection and manipulation of the magnetic order in two-dimensional antiferromagnets. Furthermore, they will overcome the difficulties with weak magnetic responses inherent in the use of antiferromagnets and hence provide a building block for future antiferromagnetic spintronics.

DOI: 10.1103/PhysRevLett.132.236302

*Introduction.*—Intrinsic magnetism in two-dimensional (2D) materials has long been sought after but believed to hardly survive due to the enhanced thermal fluctuations according to the Mermin-Wagner theorem [1]. However, the recent discovery of mechanically exfoliated Van der Waals (vdW) magnets [2,3] has revealed that the magnetic anisotropy can resist the thermal agitation and stabilize long-range magnetic order in the 2D limit at finite temperatures [4–30]. Especially, transition metal phosphorus trichalcogenides $MPX_3$ ($M =$ Mn, Fe, Ni; $X =$ S, Se) are a family of vdW antiferromagnets, and are easily exfoliatable down to the monolayer limit due to their weak vdW interlayer interaction [31]. These materials share the same honeycomb lattice structure but the bulk antiferromagnetic (AFM) phase at low temperatures varies depending on the magnetic elements [32–36]. It therefore provides an ideal platform to investigate magnetism and magnetic excitations in the 2D limit. Furthermore, compared to ferromagnets, antiferromagnets exhibit ultrafast dynamics in the terahertz regime, null stray field, and robustness against the external magnetic field perturbation [37–39]. Therefore, the investigation of these materials paves the way towards not only the fundamental understanding of 2D magnetism, but also the possibility of high-speed and compact AFM spintronic devices.

Standard methods such as magnetization measurements and neutron diffraction, which could only access macroscopic magnetic properties, are not suitable for the study of magnetic structures of atomically thin magnets [31]. Especially, antiferromagnets do not have net magnetization; direct measurement of AFM ordering using the magneto-optical Kerr effect is not available either. Although recent studies have focused on the Raman spectroscopy [31,40–46] and the second-harmonic generation [47–50] to detect the crystal symmetry lowering associated with the AFM transition, these signals often do not provide clear identification in the monolayer limit. Therefore, a comprehensive method which suits for exploring the magnetic properties of 2D antiferromagnets is highly desired.

Here, we propose an ac intrinsic magnon spin Hall current mechanically driven by surface-acoustic waves (SAWs) as a novel method to probe the magnetic structures of such 2D honeycomb antiferromagnets (see Fig. 1). Owing to extremely large mechanical flexibility of 2D materials, SAWs are ideally suited for fundamental research of them [51]. When an inhomogeneous strain is applied to 2D honeycomb magnets, a spatial modulation of exchange energies mimics the role of artificial gauge fields for magnons [52–56]. These strain gauge fields work at the

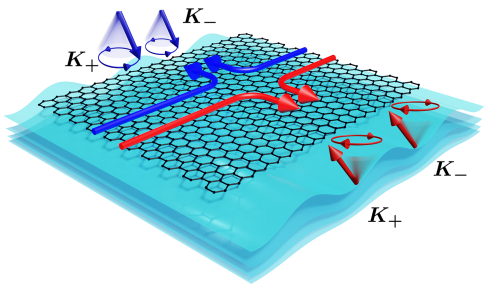


FIG. 1. Schematics of the acoustomagnonic spin Hall effect. A spatial modulation of the exchange energies due to strain mimics the role of artificial gauge fields for magnons in a honeycomb lattice. Both the strain-induced electric fields and the magnon Berry curvature work at the two valley points in the opposite direction, respectively, leading to a net spin Hall current.

 

two valley points in the opposite direction, which in turn activates the valley degrees of freedom (d.o.f.). Therefore, the valley d.o.f. with the use of SAWs is a promising concept for detection and manipulation of the magnetic order in 2D vdW antiferromagnets. Furthermore, our mechanically driven magnon spin Hall effect will overcome the difficulties with weak magnetic responses inherent in the use of antiferromagnets and hence provide a building block for more sophisticated AFM spintronics.

*Formulation.*—We start from a standard nearest-neighbor AFM Heisenberg model of spins $S$ placed on the sites of a honeycomb lattice:

$$\hat{H}_0 = J\sum_{\langle i,j\rangle}\hat{\boldsymbol{S}}_i\cdot\hat{\boldsymbol{S}}_j, \tag{1}$$

where $J>0$ is the AFM exchange interaction, $\hat{\boldsymbol{S}}_i=(\hat{S}_i^x,\hat{S}_i^y,\hat{S}_i^z)$ are the spin operators at the $i$th site, and the sum $\langle i,j\rangle$ runs over nearest-neighbor sites. Here, we have neglected the magnetic anisotropy because this entails only quantitative changes in the main results [57]. We also assume that the ground state of the unstrained Hamiltonian $\hat{H}_0$ is the Néel ordered state perpendicular to the hexagonal plane and it is maintained under weak strain.

The quantized spin-wave excitations in magnets, so-called magnons, have attracted special attention as a promising candidate for a spin information carrier with good coherence and without dissipation of the Joule heating [58–70]. The excitation spectrum of magnons is obtained by the linear spin-wave theory. We perform the Holstein-Primakoff transformation for magnons on sublattices A and B, respectively [71],

$$\hat{S}^+_{i,\mathrm{A}}=\sqrt{2S-\hat{a}_i^\dagger\hat{a}_i}\hat{a}_i,\qquad \hat{S}^z_{i,\mathrm{A}}=S-\hat{a}_i^\dagger\hat{a}_i, \tag{2a}$$

$$\hat{S}^+_{j,\mathrm{B}}=\hat{b}_j^\dagger\sqrt{2S-\hat{b}_j^\dagger\hat{b}_j},\qquad \hat{S}^z_{j,\mathrm{B}}=-S+\hat{b}_j^\dagger\hat{b}_j, \tag{2b}$$

which describe fluctuations above the Néel ordered ground state and $\hat{S}_j^\pm=\hat{S}_j^x\pm i\hat{S}_j^y$ are the raising and lowering operators for the $j$th spin. Here, the bosonic operator $\hat{a}_i$ ($\hat{b}_j^\dagger$) annihilates (creates) a magnon at the $i$ ($j$)th $A$ ($B$) site. The Hamiltonian is then diagonalized by subsequent Fourier and Bogoliubov transformations: $\hat{\alpha}_{\boldsymbol{k}}=u_{\boldsymbol{k}}\hat{a}_{\boldsymbol{k}}-v_{\boldsymbol{k}}\hat{b}^\dagger_{-\boldsymbol{k}}$ and $\hat{\beta}^\dagger_{-\boldsymbol{k}}=u_{\boldsymbol{k}}\hat{b}^\dagger_{-\boldsymbol{k}}-v^*_{\boldsymbol{k}}\hat{a}_{\boldsymbol{k}}$, and Eq. (1) is cast into noninteracting Dirac magnons [53],

$$\hat{H}_0=\sum_{\boldsymbol{k}}\left(\hbar\omega^\alpha_{\boldsymbol{k}}\hat{\alpha}^\dagger_{\boldsymbol{k}}\hat{\alpha}_{\boldsymbol{k}}+\hbar\omega^\beta_{\boldsymbol{k}}\hat{\beta}^\dagger_{\boldsymbol{k}}\hat{\beta}_{\boldsymbol{k}}\right), \tag{3}$$

which is justified well below the Néel temperature. In these honeycomb systems, two inequivalent valley points $K_\pm$ reside at the corners of the hexagonal Brillouin zone (see Fig. 2). In the vicinity of $K_\pm$, $\hat{\alpha}_{\boldsymbol{k}}$ ($\hat{\beta}_{\boldsymbol{k}}$) can be regarded as

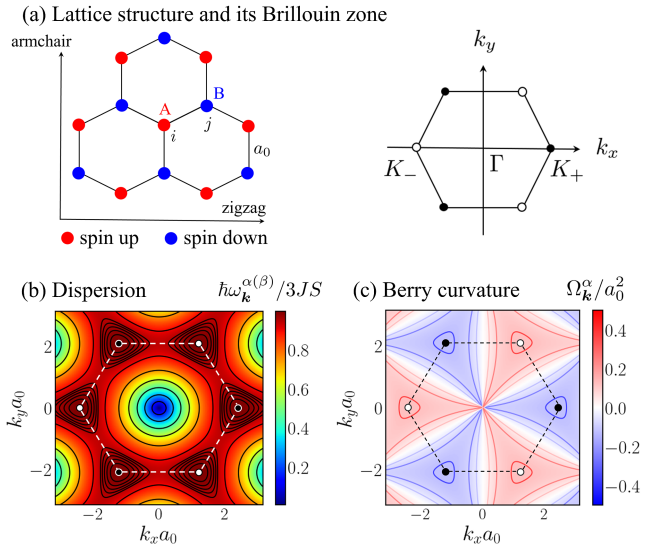


FIG. 2. (a) Lattice structure of the Néel ordered honeycomb antiferromagnets and the corresponding Brillouin zone. Two valley points $K_\pm$ reside at the corners of the hexagonal Brillouin zone. (b) Dispersion of magnons in the unstrained honeycomb Heisenberg antiferromagnets, which shows quadratic maximum at the valley points. (c) Distribution of the magnon Berry curvature for $\alpha$ magnons.

$\hat{a}_{\boldsymbol{k}}$ ($\hat{b}_{\boldsymbol{k}}$) because the Bogoliubov coefficients are approximated as $u_{K_\pm}\simeq 1$ and $v_{K_\pm}\simeq 0$. The relevant spectrum of magnons near the valley points are described by a quadratic dispersion: $\hbar\omega^{\alpha(\beta)}_{K_\pm}(\boldsymbol{q})=3JS\sqrt{1-a_0^2\boldsymbol{q}^2/4}$ with relative momentum $\boldsymbol{q}=(q_x,q_y)$ measured from the valley center. We also obtain the magnon Berry curvature $\boldsymbol{\Omega}^\alpha_{\boldsymbol{k}}=-\boldsymbol{\Omega}^\beta_{\boldsymbol{k}}$ and its distribution is depicted in Fig. 2(c). Notice that $\boldsymbol{\Omega}^\alpha_{\boldsymbol{k}}$ is an odd function and it shows opposite values in the vicinity of $K_\pm$.

A continuum model for Dirac magnons is complemented with elasticity theory [72] to incorporate the effect of strain. We here consider a spatial modulation of the exchange energies due to strain which mimics the role of artificial gauge fields that govern magnon dynamics. For large lattice, the displacement field $\boldsymbol{u}(\boldsymbol{r},t)=(u_x,u_y,u_z)$ can be taken as a smooth function of the coordinates, and the strain tensor is defined by $\varepsilon_{ij}=(\partial_i u_j+\partial_j u_i+\partial_i h\partial_j h)/2$ having $h=u_z$ as the normal component of the displacement. By expanding the operators around the two valley points: $\hat{a}(\boldsymbol{r})\simeq e^{i\boldsymbol{K}_\pm\cdot\boldsymbol{r}}\hat{\psi}_a^{K_\pm}(\boldsymbol{r})$, $\hat{b}(\boldsymbol{r})\simeq e^{-i\boldsymbol{K}_\pm\cdot\boldsymbol{r}}\hat{\psi}_b^{K_\pm}(\boldsymbol{r})$, we obtain the strained Hamiltonian as [57]

$$\hat{H}=\int d\boldsymbol{r}\,\hat{\boldsymbol{\Psi}}^\dagger(\boldsymbol{r})\begin{pmatrix}\mathcal{H}^{K_+} & 0\\ 0 & \mathcal{H}^{K_-}\end{pmatrix}\hat{\boldsymbol{\Psi}}(\boldsymbol{r}), \tag{4}$$

where $\hat{\boldsymbol{\Psi}}^\dagger=(\hat{\psi}_a^{K_+\dagger},\hat{\psi}_b^{K_+},\hat{\psi}_a^{K_-\dagger},\hat{\psi}_b^{K_-})$ and the continuous effective Hamiltonian is given by

$$\mathcal{H}^{K_\eta} = -v_J(-i\hbar\boldsymbol{\nabla} + \eta\boldsymbol{A}^s)\cdot\boldsymbol{\sigma}_\eta + 3JS - \phi^s. \tag{5}$$

$v_J = 3JSa_0/2\hbar$ is the exchange velocity of magnons with the length of the bond between neighboring magnetic atoms $a_0$. Here, $\eta = \pm 1$ is the valley index labelling the two inequivalent valleys $K_\pm$ and $\boldsymbol{\sigma}_\eta = (\eta\sigma_x, \sigma_y)$ are the Pauli matrices representing a psuedospin from the sublattice d.o.f. The vector potential $\boldsymbol{A}^s = \hbar(\gamma/2a_0)(\varepsilon_{xx} - \varepsilon_{yy}, -2\varepsilon_{xy})$ couples minimally to the magnonic excitations with opposite signs at the two valley points, which results in the activation of the valley d.o.f. The scalar potential $\phi^s = (3JS/2)\gamma(\varepsilon_{xx} + \varepsilon_{yy})$ originates from the change of density due to the variation of the sample area described by $\boldsymbol{\nabla}\cdot\boldsymbol{u}$. The factor $\gamma$ encodes the strength of the magnetoelastic coupling, which is expected to be of the order of unity [73]. Note that the emergence of the strain gauge fields is related to the fact that quasiparticles in Dirac systems are described by the corresponding relativisticlike equations [74–78].

The introduction of the gauge fields $(\phi^s, \boldsymbol{A}^s)$ leads to emergent pseudoelectromagnetic fields:

$$\boldsymbol{E}_1^s = -\boldsymbol{\nabla}\phi^s, \qquad \boldsymbol{E}_2^s = -\partial_t\boldsymbol{A}^s, \tag{6a}$$

$$\boldsymbol{B}^s = \boldsymbol{\nabla}\times\boldsymbol{A}^s. \tag{6b}$$

Here, $\boldsymbol{E}_2^s$ is generated only when considering a time-varying strain such as SAWs and has a significant importance for the main results. Fundamentally, this pseudoelectric field couples not the charge d.o.f. but the valley, and hence opens a new paradigm to explore novel properties of charge-neutral quasiparticles [79–81]. Previous magnon transport in conventional antiferromagnets relies on thermal gradients as a driving force [82–87], but these alone cannot distinguish the spin between two magnons; therefore, a magnon-mediated spin current has been difficult to generate without lifting the degeneracy of two magnons. However, in honeycomb antiferromagnets, the valley d.o.f. is activated by the strain gauge fields and hence has a potential to result in a pure spin current by combining with the valley-contrasting magnon Berry curvature.

The semiclassical equations for magnons under strain-induced pseudoelectromagnetic fields Eq. (6) are derived in a similar form to the conventional semiclassical equations for electrons [88],

$$\dot{\boldsymbol{r}}_\eta^{\alpha(\beta)} = \frac{\partial\omega_\eta^{\alpha(\beta)}}{\partial\boldsymbol{q}} - \dot{\boldsymbol{q}}_\eta^{\alpha(\beta)}\times\boldsymbol{\Omega}_\eta^{\alpha(\beta)}, \tag{7a}$$

$$\hbar\dot{\boldsymbol{q}}_\eta^{\alpha(\beta)} = -\boldsymbol{E}_\eta^s - \dot{\boldsymbol{r}}_\eta^{\alpha(\beta)}\times\boldsymbol{B}_\eta^s, \tag{7b}$$

where we have introduced a compact form of pseudoelectromagnetic fields: $\boldsymbol{B}_\eta^s = \eta\boldsymbol{B}^s$, $\boldsymbol{E}_\eta^s = \boldsymbol{E}_1^s + \eta\boldsymbol{E}_2^s$. We should note the validity of the treatment in the framework of the semiclassical approach. The typical frequencies of SAWs range from MHz to GHz, whereas those of relevant magnons in the vicinity of valley points are of the order of THz; therefore, we can assume that magnons adiabatically follow the deformation and their dynamics are governed by Eq. (7).

*Rayleigh-type SAWs-induced pseudoelectric fields.*— Among the diverse modes of SAWs, the Rayleigh-type waves, which are the superposition of longitudinal and normal components, can be easily excited under traction-free boundary conditions on piezoelectric substrates [51]. Considering Rayleigh-type SAWs propagating on the surface of a piezoelectric substrate in the $xy$ plane (see Fig. 3), the displacement field is given by

$$\boldsymbol{u}_{\text{Rayleigh}}(\boldsymbol{r}, t) = \text{Re}[(u_L\hat{\boldsymbol{Q}} + iu_z\hat{\boldsymbol{z}})e^{i(\boldsymbol{Q}\cdot\boldsymbol{r}-\omega t)}], \tag{8}$$

where $u_L$ and $u_z$ are the longitudinal and normal displacements, $\boldsymbol{Q} = Q(\cos\theta, \sin\theta)$ is the in-plane propagating wave vector with $\theta$ being an azimuthal angle, and $\omega$ is the frequency of applying SAWs. Here, $\theta = 0$ corresponds to the $x$ direction with the zigzag orientation of the honeycomb lattice. By assuming that the Van der Waals magnet on a piezoelectric substrate completely follows the displacement of the substrate, the Rayleigh-type SAWs-induced pseudoelectric fields reads

$$\boldsymbol{E}_2^s = \hbar\frac{\gamma}{2a_0}c_t\xi Q^2\text{Re}[u_L(-\cos 3\theta\hat{\boldsymbol{Q}} + \sin 3\theta\hat{\boldsymbol{\theta}})e^{i(\boldsymbol{Q}\cdot\boldsymbol{r}-\omega t)}], \tag{9}$$

where $\hat{\boldsymbol{\theta}} = \partial_\theta\hat{\boldsymbol{Q}} = (-\sin\theta, \cos\theta)$ is the azimuthal unit vector transverse to $\hat{\boldsymbol{Q}}$, $c_t$ is the transverse velocity of the sound wave, and $\xi$ is a constant characterizing the SAWs dispersion as $\omega = c_t\xi Q$. We should note that the pseudoelectromagnetic fields stemming from the out-of-plane displacement are proportional to $u_z^2$ due to $\partial_i h\partial_j h$, which is less relevant under weak strain, and hence we neglect their contributions in the following analysis.

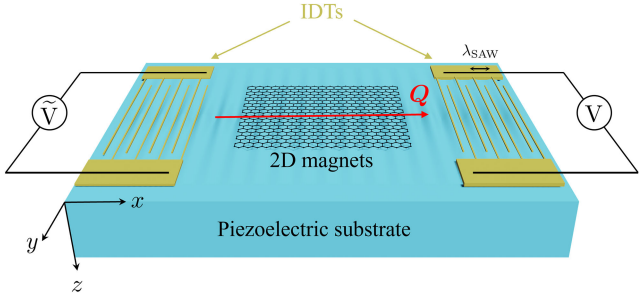


FIG. 3. Schematic illustration of the Rayleigh-type SAWs generation. SAWs are mainly generated, detected, and controlled by interdigital transducers (IDTs) placed on the ends of a piezoelectric substrate. IDTs are periodic arrays of metallic finger electrodes with a pitch of half the SAW wavelength $\lambda_{\text{SAW}} = 2\pi/Q$ and convert ac electric signals into the SAWs propagating along $\boldsymbol{Q}$ via the inverse piezoelectric effect.

*Acoustomagnonic spin Hall effect.*—As a demonstration of semiclassical magnon transport driven by SAWs-induced gauge fields, we consider magnon-mediated spin currents. Because the two valley points are largely separated in the Brillouin zone, the valley index $\eta$ can be used as a good quantum number in the presence of weak disorder. In previous works, various electron transport phenomena under strain applied to 2D Dirac materials have been intensively studied [89–98]. However, the role of SAWs in magnon transport has not been well investigated yet.

Since the two magnons are completely decoupled in Eq. (3), we can treat the dynamics of each mode independently. The Boltzmann equation for $\alpha(\beta)$ magnons is then given by

$$\frac{\partial n_\eta^{\alpha(\beta)}}{\partial t}+\dot{\boldsymbol{r}}_\eta\cdot\frac{\partial n_\eta^{\alpha(\beta)}}{\partial \boldsymbol{r}}+\dot{\boldsymbol{q}}_\eta\cdot\frac{\partial n_\eta^{\alpha(\beta)}}{\partial \boldsymbol{q}}=-\frac{n_\eta^{\alpha(\beta)}-n_{\mathrm{B}}(\hbar\omega_{\boldsymbol{q}})}{\tau}, \tag{10}$$

where $n_\eta^{\alpha(\beta)}(\boldsymbol{r},\boldsymbol{q},t)$ is the distribution function for $\alpha$ ($\beta$) magnons with valley $\eta$ and relative momentum $\boldsymbol{q}$. $n_{\mathrm{B}}(\epsilon)=(e^{\epsilon/k_{\mathrm{B}}T}-1)^{-1}$ is the Bose-Einstein distribution function with zero chemical potential and $\tau$ is the momentum relaxation time for magnons.

We are now ready to discuss the magnon-mediated spin currents driven by the Rayleigh-type SAWs. By invoking the Bogoliubov transformation, we obtain the $z$ component of the total spin as $\hbar\sum_{\boldsymbol{k}}(-\hat{\alpha}_{\boldsymbol{k}}^\dagger\hat{\alpha}_{\boldsymbol{k}}+\hat{\beta}_{\boldsymbol{k}}^\dagger\hat{\beta}_{\boldsymbol{k}})$, and thereby $-\hbar$ ($+\hbar$) spin angular momentum is carried by $\alpha$ ($\beta$) magnons [99]. Because the strain gauge fields only work around the two valley points and magnons in other points do not contribute to the spin currents due to their degeneracy [57], we only consider the contribution from the vicinity of $K_\pm$:

$$\boldsymbol{j}_{\mathrm{s}}^z=\hbar\sum_{\eta=\pm1}\int[\mathrm{d}\boldsymbol{q}](-\mathcal{D}^\alpha\dot{\boldsymbol{r}}_\eta^\alpha n_\eta^\alpha+\mathcal{D}^\beta\dot{\boldsymbol{r}}_\eta^\beta n_\eta^\beta), \tag{11}$$

where the factor $\mathcal{D}^{\alpha(\beta)}\equiv1+(1/\hbar)\boldsymbol{B}_\eta^s\cdot\boldsymbol{\Omega}_\eta^{\alpha(\beta)}(\boldsymbol{q})$ is a field-induced correction to the volume of the phase space and $\int[\mathrm{d}\boldsymbol{q}]\equiv\int\mathrm{d}^2\boldsymbol{q}/(2\pi)^2$. By substituting Eq. (7) into Eq. (11), we obtain a transverse magnon-mediated spin current as

$$\begin{aligned}\boldsymbol{j}_{\mathrm{s}}^z&=\boldsymbol{E}_2^s\times\int[\mathrm{d}\boldsymbol{q}](-\boldsymbol{\Omega}_+^\alpha n_+^\alpha+\boldsymbol{\Omega}_-^\alpha n_-^\alpha+\boldsymbol{\Omega}_+^\beta n_+^\beta-\boldsymbol{\Omega}_-^\beta n_-^\beta)\\&=-\boldsymbol{E}_2^s\times\int[\mathrm{d}\boldsymbol{q}]\boldsymbol{\Omega}_+^\alpha(n_+^\alpha+n_-^\alpha+n_+^\beta+n_-^\beta),\end{aligned} \tag{12}$$

where we have used the relation $\boldsymbol{\Omega}_{\boldsymbol{k}}^\alpha=-\boldsymbol{\Omega}_{-\boldsymbol{k}}^\alpha=-\boldsymbol{\Omega}_{\boldsymbol{k}}^\beta$ [100]. Equation (12) is the main result of this Letter, which originates from the interplay between the strain gauge fields and the magnon Berry curvature. Both of them have a valley-contrasting property and work in the opposite direction at the two valley points respectively, resulting in a net spin Hall current (see Fig. 1). Furthermore, Eq. (12) gives a finite contribution even when the magnons obey the Bose-Einstein distribution $n_{\mathrm{B}}$; therefore, our mechanically driven spin Hall current dubbed acoustomagnonic spin Hall effect becomes independent of the magnon relaxation time $\tau$ and hence provides an intrinsic spin Hall current.

*Discussion.*—Finally, we will discuss the experimental feasibility of our acoustomagnonic spin Hall effect. Transition metal phosphorus trichalcogenides $MPX_3$ are a family of AFM semiconductors with a band gap of the order of 1 eV [11–15], which is much larger than the typical frequency of SAWs, and hence the spin transport is dominated by magnons. Here, we suppose $MnPS_3$ as a candidate of Néel-type antiferromagnets [45–48], in which long-distance magnon transport over several micrometers has been recently observed [101]. By introducing the cutoff wave number $q_c$, which is a radius of the effective region of strain gauge fields in the vicinity of each valley point, the spin Hall conductivity is approximated as

$$\begin{aligned}\sigma_s^{\mathrm{AMHE}}&=\int_{3JS\sqrt{1-a_0^2q_c^2/4}}^{3JS}\mathrm{d}\epsilon\,D(\epsilon)\Omega^\alpha(\epsilon)n_{\mathrm{B}}(\epsilon)\\&\simeq\frac{q_c^2a_0^2}{4\pi}\frac{1}{e^{3JS/k_{\mathrm{B}}T}-1},\end{aligned} \tag{13}$$

where $D(\epsilon)$ is the density of states and we have defined the spin Hall conductivity owing to acoustomagnonic spin Hall effect as $\boldsymbol{j}_s^z=\sigma_s^{\mathrm{AMHE}}\boldsymbol{E}_2^s\times\hat{\boldsymbol{z}}$. Figure 4 shows the temperature and $q_c$ dependences of $\sigma_s^{\mathrm{AMHE}}$, in which the horizontal axis is normalized by $3JS/k_{\mathrm{B}}\simeq134$ K. The Néel temperature is experimentally obtained as $T_{\mathrm{N}}\simeq79$ K [48,101]. Therefore, the amplitude of the spin current $|\boldsymbol{j}_s^z|$ is estimated to be of the order of meV/m at $T\ll T_{\mathrm{N}}$ with the pseudoelectric field $|\boldsymbol{E}_2^s|\simeq1$ eV/m induced by the Rayleigh-type SAWs. Here, we have used the parameters [101]: $J\simeq1.54$ meV, $S=5/2$, $a_0\sim1$ Å, $u_L\simeq100$ pm, $\lambda_{\mathrm{SAW}}=2\pi/Q\simeq1$ μm, $c_t=4000$ m/s, $\xi\simeq0.95$, and

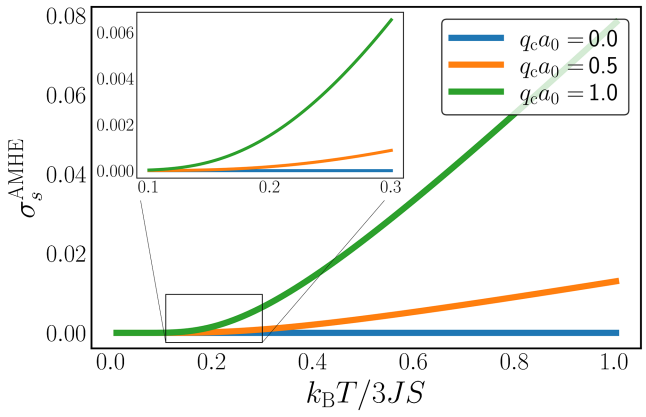


FIG. 4. Temperature dependence of the acoustomagnonic spin Hall conductivity $\sigma_s^{\mathrm{AMHE}}$ for different values of $q_ca_0$. The horizontal axis is normalized by $3JS/k_{\mathrm{B}}$.

$\gamma \sim 1$ [73]. This ac spin current oscillating in the order of GHz may be detected by the present experiments such as spin wave resonance [102,103].

The conventional strategy for generating magnon spin currents in AMF spintronics has been applying magnetic fields in order to lift the degeneracy of magnons or to realize a canted AFM structure along the fields [37–39]. This provides only weak spin currents due to extrinsically perturbative magnetic fields. On the other hand, the valley d.o.f., which is a characteristic of the honeycomb lattice structure, is activated by the strain-induced gauge fields. Here, we have focused on the interplay between the strain gauge fields and the magnon Berry curvature, which have opposite sign between the two valley points respectively, resulting in an intrinsic magnon spin Hall current. This fact may offer a bright prospect for the long-standing dilemma that antiferromagnets show only weak magnetic responses which are hard to detect and control. Furthermore, our acoustomagnonic spin Hall effect does not require the Dzyaloshinskii-Moriya interaction, which is an essential ingredient for the magnon spin Nernst effect [82–84] but is negligible in $MnPS_3$ [104]. In addition, our results do not rely on the nontrivial topology of magnon bands originating from the magnon-phonon coupling. However, the magnon-phonon coupling results in the formation of the hybridized excitation of magnons and phonons, which can carry large Berry curvature in the anticrossing regions between their bands [105–109]. The impact of the magnon-phonon coupling on our results may be an interesting future work. Therefore, our results will overcome the difficulties inherent in the use of antiferromagnets and provide a building block for more sophisticated AFM spintronics.

Symmetry considerations are summarized in Table I. We can see that the symmetry of $\boldsymbol{E}_2^s$ is quite different from that of the conventional thermal gradient. Thus, $\boldsymbol{E}_2^s$-induced magnon spin currents are prohibited in centrosymmetric antiferromagnets and our acoustomagnonic spin Hall effect becomes a novel probe for noncentrosymmetric AFM phases such as the Néel ordered phase. Furthermore, $\boldsymbol{E}_2^s$ can generate magnon spin current with preserving the effective time reversal symmetry $\mathcal{TC}$, which is the combined action of time reversal $\mathcal{T}$ and 180° spin rotation around an in-plane axis $\mathcal{C}$. This is why our acoustomagnonic spin Hall effect does not require the Dzyaloshinskii-Moriya interaction and the magnon-phonon coupling.

TABLE I. Symmetry classification and comparison of the conventional thermal gradient and the strain-induced pseudoelectric fields introduced in this work under the inversion $\mathcal{P}$, the time reversal $\mathcal{T}$, and the effective time reversal $\mathcal{TC}$ symmetry operations.

| Input and output fields | | $\mathcal{P}$ | $\mathcal{T}$ | $\mathcal{TC}$ |
|---|---|---|---|---|
| Thermal gradient | $\boldsymbol{\nabla} T$ | − | + | + |
| Strain tensor | $\varepsilon_{ij}$ | + | + | + |
| Strain gauge fields | $\phi^s$, $\boldsymbol{A}^s$ | + | + | + |
| Pseudoelectric field | $\boldsymbol{E}_2^s$ | + | − | − |
| Magnon spin current | $\boldsymbol{j}_s^z$ | − | + | − |

*Conclusion.*—In summary, we have developed a basic framework of SAWs-driven magnon transport in a honeycomb antiferromagnet. Here, we have proposed a magnon-mediated spin Hall current driven by the Rayleigh-type SAWs dubbed acoustomagnonic spin Hall effect as a novel probe for exploring the magnetic properties of such 2D vdW antiferromagnets. By focusing on the valley d.o.f., we have revealed that the interplay between the strain gauge fields and the magnon Berry curvature results in an intrinsic spin Hall current without the Dyzaloshinskii-Moriya interaction and the magnon-phonon coupling in the Néel ordered state. Therefore, our results open a promising route for mechanical detection and manipulation of the magnetic order in 2D antiferromagnets. Furthermore, they will overcome the difficulties with weak magnetic responses inherent in the use of antiferromagnets and hence provide a building block for future AFM spintronics. Recent studies have shown that the strain effect also introduces the pseudogauge fields for Dirac magnons in honeycomb ferromagnets [52], twisted honeycomb ferromagnet [54], and honeycomb noncollinear antiferromagnets [110]. Therefore, magnon Hall effects driven by the surface acoustic waves may be applicable to a wide range of 2D magnets and are our interesting future work. Furthermore, we expect that the measurements of the magnon Hall effect based on our strategy is robust against electronic contributions [111]. Our work motivates further systematic studies on 2D vdW magnets, which are significant not only for the potentially diverse applications, but also for the fundamental understanding of 2D magnetism.

The authors are grateful to K. Shinada, M. Chazono, S. Kaneshiro, T. Funato, J. Fujimoto, and D. Oue for valuable discussions. R. S. thanks Y. Nozaki, K. Yamanoi, T. Horaguchi, S. Watanabe, and S. Fujii for providing helpful comments from an experimental point of view. We also thank the referees for noticing Refs. [105–109]. R. S. is supported by JSPS KAKENHI (Grants No. JP 22J20221 and No. 22KJ1937). This work was supported by the Priority Program of Chinese Academy of Sciences under Grant No. XDB28000000, and by JSPS KAKENHI for Grants (No. 20H01863, No. 21H04565, and No. 23H01839) from MEXT, Japan.

*sano.ryotaro.52v@st.kyoto-u.ac.jp

[1] N. D. Mermin and H. Wagner, Absence of ferromagnetism or antiferromagnetism in one- or two-dimensional isotropic Heisenberg models, Phys. Rev. Lett. **17**, 1133 (1966).

[2] Cheng Gong, Lin Li, Zhenglu Li, Huiwen Ji, Alex Stern, Yang Xia, Ting Cao, Wei Bao, Chenzhe Wang, Yuan

Wang, Z. Q. Qiu, R. J. Cava, Steven G. Louie, Jing Xia, and Xiang Zhang, Discovery of intrinsic ferromagnetism in two-dimensional van der Waals crystals, Nature (London) **546**, 265 (2017).

[3] Bevin Huang, Genevieve Clark, Efrén Navarro-Moratalla, Dahlia R. Klein, Ran Cheng, Kyle L. Seyler, Ding Zhong, Emma Schmidgall, Michael A. McGuire, David H. Cobden, Wang Yao, Di Xiao, Pablo Jarillo-Herrero, and Xiaodong Xu, Layer-dependent ferromagnetism in a van der Waals crystal down to the monolayer limit, Nature (London) **546**, 270 (2017).

[4] Kenneth S. Burch, David Mandrus, and Je-Geun Park, Magnetism in two-dimensional van der Waals materials, Nature (London) **563**, 47 (2018).

[5] Cheng Gong and Xiang Zhang, Two-dimensional magnetic crystals and emergent heterostructure devices, Science **363**, eaav4450 (2019).

[6] M. Gibertini, M. Koperski, A. F. Morpurgo, and K. S. Novoselov, Magnetic 2D materials and heterostructures, Nat. Nanotechnol. **14**, 408 (2019).

[7] Kin Fai Mak, Jie Shan, and Daniel C. Ralph, Probing and controlling magnetic states in 2D layered magnetic materials, Nat. Rev. Phys. **1**, 646 (2019).

[8] Bevin Huang, Michael A. McGuire, Andrew F. May, Di Xiao, Pablo Jarillo-Herrero, and Xiaodong Xu, Emergent phenomena and proximity effects in two-dimensional magnets and heterostructures, Nat. Mater. **19**, 1276 (2020).

[9] David L. Cortie, Grace L. Causer, Kirrily C. Rule, Helmut Fritzsche, Wolfgang Kreuzpaintner, and Frank Klose, Two-dimensional magnets: Forgotten history and recent progress towards spintronic applications, Adv. Funct. Mater. **30**, 1901414 (2020).

[10] Shuqing Zhang, Runzhang Xu, Nannan Luo, and Xiaolong Zou, Two-dimensional magnetic materials: Structures, properties and external controls, Nanoscale **13**, 1398 (2021).

[11] Mauro Och, Marie-Blandine Martin, Bruno Dlubak, Pierre Seneor, and Cecilia Mattevi, Synthesis of emerging 2D layered magnetic materials, Nanoscale **13**, 2157 (2021).

[12] Xue Jiang, Qinxi Liu, Jianpei Xing, Nanshu Liu, Yu Guo, Zhifeng Liu, and Jijun Zhao, Recent progress on 2D magnets: Fundamental mechanism, structural design and modification, Appl. Phys. Rev. **8**, 031305 (2021).

[13] Hang Xu, Shengjie Xu, Xun Xu, Jincheng Zhuang, Weichang Hao, and Yi Du, Recent advances in two-dimensional van der Waals magnets, Microstructures **2**, 2022011 (2022).

[14] Qing Hua Wang *et al.*, The magnetic genome of two-dimensional van der waals materials, ACS Nano **16**, 6960 (2022).

[15] Hidekazu Kurebayashi, Jose H. Garcia, Safe Khan, Jairo Sinova, and Stephan Roche, Magnetism, symmetry and spin transport in van der Waals layered systems, Nat. Rev. Phys. **4**, 150 (2022).

[16] Bevin Huang, Genevieve Clark, Dahlia R. Klein, David MacNeill, Efrén Navarro-Moratalla, Kyle L. Seyler, Nathan Wilson, Michael A. McGuire, David H. Cobden, Di Xiao, Wang Yao, Pablo Jarillo-Herrero, and Xiaodong Xu, Electrical control of 2D magnetism in bilayer $CrI_3$, Nat. Nanotechnol. **13**, 544 (2018).

[17] Shengwei Jiang, Jie Shan, and Kin Fai Mak, Electric-field switching of two-dimensional van der Waals magnets, Nat. Mater. **17**, 406 (2018).

[18] Shengwei Jiang, Lizhong Li, Zefang Wang, Kin Fai Mak, and Jie Shan, Controlling magnetism in 2D $CrI_3$ by electrostatic doping, Nat. Nanotechnol. **13**, 549 (2018).

[19] Tiancheng Song, Xinghan Cai, Matisse Wei-Yuan Tu, Xiaoou Zhang, Bevin Huang, Nathan P. Wilson, Kyle L. Seyler, Lin Zhu, Takashi Taniguchi, Kenji Watanabe, Michael A. McGuire, David H. Cobden, Di Xiao, Wang Yao, and Xiaodong Xu, Giant tunneling magnetoresistance in spin-filter van der Waals heterostructures, Science **360**, 1214 (2018).

[20] Baishun Yang, Xiaolin Zhang, Hongxin Yang, Xiufeng Han, and Yu Yan, Strain controlling transport properties of heterostructure composed of monolayer $CrI_3$, Appl. Phys. Lett. **114**, 192405 (2019).

[21] Tiancheng Song, Zaiyao Fei, Matthew Yankowitz, Zhong Lin, Qianni Jiang, Kyle Hwangbo, Qi Zhang, Bosong Sun, Takashi Taniguchi, Kenji Watanabe, Michael A. McGuire, David Graf, Ting Cao, Jiun-Haw Chu, David H. Cobden, Cory R. Dean, Di Xiao, and Xiaodong Xu, Switching 2D magnetic states via pressure tuning of layer stacking, Nat. Mater. **18**, 1298 (2019).

[22] Weijong Chen, Zeyuan Sun, Zhongjie Wang, Lehua Gu, Xiaodong Xu, Shiwei Wu, and Chunlei Gao, Direct observation of van der Waals stacking-dependent interlayer magnetism, Science **366**, 983 (2019).

[23] Chenhao Jin, Zui Tao, Kaifei Kang, Kenji Watanabe, Takashi Taniguchi, Kin Fai Mak, and Jie Shan, Imaging and control of critical fluctuations in two-dimensional magnets, Nat. Mater. **19**, 1290 (2020).

[24] Zaiyao Fei, Bevin Huang, Paul Malinowski, Wenbo Wang, Tiancheng Song, Joshua Sanchez, Wang Yao, Di Xiao, Xiaoyang Zhu, Andrew F. May, Weida Wu, David H. Cobden, Jiun-Haw Chu, and Xiaodong Xu, Two-dimensional itinerant ferromagnetism in atomically thin $Fe_3GeTe_2$, Nat. Mater. **17**, 778 (2018).

[25] Yujun Deng, Yijun Yu, Yichen Song, Jingzhao Zhang, Nai Zhou Wang, Zeyuan Sun, Yangfan Yi, Yi Zheng Wu, Shiwei Wu, Junyi Zhu, Jing Wang, Xian Hui Chen, and Yuanbo Zhang, Gate-tunable room-temperature ferromagnetism in two-dimensional $Fe_3GeTe_2$, Nature (London) **563**, 94 (2018).

[26] D. R. Klein, D. MacNeill, J. L. Lado, D. Soriano, E. Navarro-Moratalla, K. Watanabe, T. Taniguchi, S. Manni, P. Canfield, J. Fernández-Rossier, and P. Jarillo-Herrero, Probing magnetism in 2D van der Waals crystalline insulators via electron tunneling, Science **360**, 1218 (2018).

[27] Zhe Wang, Marco Gibertini, Dumitru Dumcenco, Takashi Taniguchi, Kenji Watanabe, Enrico Giannini, and Alberto F. Morpurgo, Determining the phase diagram of atomically thin layered antiferromagnet $CrCl_3$, Nat. Nanotechnol. **14**, 1116 (2019).

[28] Zhaowei Zhang, Jingzhi Shang, Chongyun Jiang, Abdullah Rasmita, Weibo Gao, and Ting Yu, Direct photoluminescence probing of ferromagnetism in monolayer two-dimensional $CrBr_3$, Nano Lett. **19**, 3138 (2019).

[29] M. Kim, P. Kumaravadivel, J. Birkbeck, W. Kuang, S. G. Xu, D. G. Hopkinson, J. Knolle, P. A. McClarty, A. I. Berdyugin, M. Ben Shalom, R. V. Gorbachev, S. J. Haigh, S. Liu, J. H. Edgar, K. S. Novoselov, I. V. Grigorieva, and A. K. Geim, Micromagnetometry of two-dimensional ferromagnets, National electronics review **2**, 457 (2019).

[30] Anike Purbawati, Johann Coraux, Jan Vogel, Abdellali Hadj-Azzem, NianJheng Wu, Nedjma Bendiab, David Jegouso, Julien Renard, Laetitia Marty, Vincent Bouchiat, André Sulpice, Lucia Aballe, Michael Foerster, Francesca Genuzio, Andrea Locatelli, Tevfik Onur Menteş, Zheng Vitto Han, Xingdan Sun, Manuel Núñez-Regueiro, and Nicolas Rougemaille, In-plane magnetic domains and néel-like domain walls in thin flakes of the room temperature $CrTe_2$ van der Waals ferromagnet, ACS Appl. Mater. Interfaces **12**, 30702 (2020).

[31] Ke-zhao Du, Xing-zhi Wang, Yang Liu, Peng Hu, M. Iqbal Bakti Utama, Chee Kwan Gan, Qihua Xiong, and Christian Kloc, Weak van der Waals stacking, wide-range band gap, and Raman study on ultrathin layers of metal phosphorus trichalcogenides, ACS Nano **10**, 1738 (2016).

[32] P. A. Joy and S. Vasudevan, Magnetism in the layered transition-metal thiophosphates $MPS_3$ ($M$ = Mn, Fe, and Ni), Phys. Rev. B **46**, 5425 (1992).

[33] E. Ressouche, M. Loire, V. Simonet, R. Ballou, A. Stunault, and A. Wildes, Magnetoelectric $MnPS_3$ as a candidate for ferrotoroidicity, Phys. Rev. B **82**, 100408(R) (2010).

[34] A. R. Wildes, V. Simonet, E. Ressouche, G. J. McIntyre, M. Avdeev, E. Suard, S. A. J. Kimber, D. Lançon, G. Pepe, B. Moubaraki, and T. J. Hicks, Magnetic structure of the quasi-two-dimensional antiferromagnet $NiPS_3$, Phys. Rev. B **92**, 224408 (2015).

[35] D. Lançon, R. A. Ewings, T. Guidi, F. Formisano, and A. R. Wildes, Magnetic exchange parameters and anisotropy of the quasi-two-dimensional antiferromagnet $NiPS_3$, Phys. Rev. B **98**, 134414 (2018).

[36] Gen Long, Hugo Henck, Marco Gibertini, Dumitru Dumcenco, Zhe Wang, Takashi Taniguchi, Kenji Watanabe, Enrico Giannini, and Alberto F. Morpurgo, Persistence of magnetism in atomically thin $MnPS_3$ crystals, Nano Lett. **20**, 2452 (2020).

[37] T. Jungwirth, X. Marti, P. Wadley, and J. Wunderlich, Antiferromagnetic spintronics, Nat. Nanotechnol. **11**, 231 (2016).

[38] V. Baltz, A. Manchon, M. Tsoi, T. Moriyama, T. Ono, and Y. Tserkovnyak, Antiferromagnetic spintronics, Rev. Mod. Phys. **90**, 015005 (2018).

[39] Danrong Xiong, Yuhao Jiang, Kewen Shi, Ao Du, Yuxuan Yao, Zongxia Guo, Daoqian Zhu, Kaihua Cao, Shouzhong Peng, Wenlong Cai, Dapeng Zhu, and Weisheng Zhao, Antiferromagnetic spintronics: An overview and outlook, Fundam. Res. **2**, 522 (2022).

[40] Cheng-Tai Kuo, Michael Neumann, Karuppannan Balamurugan, Hyun Ju Park, Soonmin Kang, Hung Wei Shiu, Jin Hyoun Kang, Byung Hee Hong, Moonsup Han, Tae Won Noh, and Je-Geun Park, Exfoliation and Raman spectroscopic fingerprint of few-layer $NiPS_3$ van der Waals crystals, Sci. Rep. **6**, 20904 (2016).

[41] Jae-Ung Lee, Sungmin Lee, Ji Hoon Ryoo, Soonmin Kang, Tae Yun Kim, Pilkwang Kim, Cheol-Hwan Park, Je-Geun Park, and Hyeonsik Cheong, Ising-type magnetic ordering in atomically thin $FePS_3$, Nano Lett. **16**, 7433 (2016).

[42] Xingzhi Wang, Kezhao Du, Yu Yang Fredrik Liu, Peng Hu, Jun Zhang, Qing Zhang, Man Hon Samuel Owen, Xin Lu, Chee Kwan Gan, Pinaki Sengupta, Christian Kloc, and Qihua Xiong, Raman spectroscopy of atomically thin two-dimensional magnetic iron phosphorus trisulfide ($FePS_3$) crystals, 2D Mater. **3**, 031009 (2016).

[43] Amber McCreary, J. R. Simpson, T. T. Mai, R. D. McMichael, J. E. Douglas, N. Butch, C. Dennis, R. Valdés Aguilar, and A. R. Hight Walker, Quasi-two-dimensional magnon identification in antiferromagnetic $FePs_3$ via magneto-Raman spectroscopy, Phys. Rev. B **101**, 064416 (2020).

[44] Ping Liu, Zilong Xu, Haoliang Huang, Jing Li, Chao Feng, Meng Huang, Mo Zhu, Zhongping Wang, Zengming Zhang, Dazhi Hou, Yalin Lu, and Bin Xiang, Exploring the magnetic ordering in atomically thin antiferromagnetic mnpse3 by raman spectroscopy, J. Alloys Compd. **828**, 154432 (2020).

[45] Yu-Jia Sun, Qing-Hai Tan, Xue-Lu Liu, Yuan-Fei Gao, and Jun Zhang, Probing the magnetic ordering of antiferromagnetic $MnPS_3$ by Raman spectroscopy, J. Phys. Chem. Lett. **10**, 3087 (2019).

[46] Kangwon Kim, Soo Yeon Lim, Jungcheol Kim, Jae-Ung Lee, Sungmin Lee, Pilkwang Kim, Kisoo Park, Suhan Son, Cheol-Hwan Park, Je-Geun Park, and Hyeonsik Cheong, Antiferromagnetic ordering in van der Waals 2D magnetic material $MnPS_3$ probed by raman spectroscopy, 2D Mater. **6**, 041001 (2019).

[47] Hao Chu, Chang Jae Roh, Joshua O. Island, Chen Li, Sungmin Lee, Jingjing Chen, Je-Geun Park, Andrea F. Young, Jong Seok Lee, and David Hsieh, Linear magnetoelectric phase in ultrathin $MnPS_3$ probed by optical second harmonic generation, Phys. Rev. Lett. **124**, 027601 (2020).

[48] Zhuoliang Ni, Huiqin Zhang, David A. Hopper, Amanda V. Haglund, Nan Huang, Deep Jariwala, Lee C. Bassett, David G. Mandrus, Eugene J. Mele, Charles L. Kane, and Liang Wu, Direct imaging of antiferromagnetic domains and anomalous layer-dependent mirror symmetry breaking in atomically thin $MnPS_3$, Phys. Rev. Lett. **127**, 187201 (2021).

[49] Zeyuan Sun, Yangfan Yi, Tiancheng Song, Genevieve Clark, Bevin Huang, Yuwei Shan, Shuang Wu, Di Huang, Chunlei Gao, Zhanghai Chen, Michael McGuire, Ting Cao, Di Xiao, Wei-Tao Liu, Wang Yao, Xiaodong Xu, and Shiwei Wu, Giant nonreciprocal second-harmonic generation from antiferromagnetic bilayer $CrI_3$, Nature (London) **572**, 497 (2019).

[50] Zhuoliang Ni, A. V. Haglund, H. Wang, B. Xu, C. Bernhard, D. G. Mandrus, X. Qian, E. J. Mele, C. L. Kane, and Liang Wu, Imaging the Néel vector switching in the monolayer antiferromagnet $MnPSe_3$ with strain-controlled Ising order, Nat. Nanotechnol. **16**, 782 (2021).

[51] Xuchen Nie, Xiaoyue Wu, Yang Wang, Siyuan Ban, Zhihao Lei, Jiabao Yi, Ying Liu, and Yanpeng Liu, Surface acoustic wave induced phenomena in two-dimensional materials, Nanoscale Horiz. **8**, 158 (2023).

[52] Yago Ferreiros and María A. H. Vozmediano, Elastic gauge fields and Hall viscosity of Dirac magnons, Phys. Rev. B **97**, 054404 (2018).
[53] Mary Madelynn Nayga, Stephan Rachel, and Matthias Vojta, Magnon Landau levels and emergent supersymmetry in strained antiferromagnets, Phys. Rev. Lett. **123**, 207204 (2019).
[54] Tianyu Liu and Zheng Shi, Strain-induced dispersive Landau levels: Application in twisted honeycomb magnets, Phys. Rev. B **103**, 144420 (2021).
[55] Junsong Sun, Nvsen Ma, Tao Ying, Huaiming Guo, and Shiping Feng, Quantum Monte Carlo study of honeycomb antiferromagnets under a triaxial strain, Phys. Rev. B **104**, 125117 (2021).
[56] Junsong Sun, Huaiming Guo, and Shiping Feng, Magnon Landau levels in the strained antiferromagnetic honeycomb nanoribbons, Phys. Rev. Res. **3**, 043223 (2021).
[57] See Supplemental Material at http://link.aps.org/supplemental/10.1103/PhysRevLett.132.236302 for the effect of the magnetic anisotropy, the detailed derivation of the effective Hamiltonian under strain, and detailed calculations.
[58] Ken-ichi Uchida, Hiroto Adachi, Takeru Ota, Hiroyasu Nakayama, Sadamichi Maekawa, and Eiji Saitoh, Observation of longitudinal spin-Seebeck effect in magnetic insulators, Appl. Phys. Lett. **97**, 172505 (2010).
[59] V. V. Kruglyak, S. O. Demokritov, and D. Grundler, Magnonics, J. Phys. D **43**, 264001 (2010).
[60] A. A. Serga, A. V. Chumak, and B. Hillebrands, YIG magnonics, J. Phys. D **43**, 264002 (2010).
[61] Y. Kajiwara, K. Harii, S. Takahashi, J. Ohe, K. Uchida, M. Mizuguchi, H. Umezawa, H. Kawai, K. Ando, K. Takanashi, S. Maekawa, and E. Saitoh, Transmission of electrical signals by spin-wave interconversion in a magnetic insulator, Nature (London) **464**, 262 (2010).
[62] A. V. Chumak, V. I. Vasyuchka, A. A. Serga, and B. Hillebrands, Magnon spintronics, Nat. Phys. **11**, 453 (2015).
[63] YoshiChika Otani, Masashi Shiraishi, Akira Oiwa, Eiji Saitoh, and Shuichi Murakami, Spin conversion on the nanoscale, Nat. Phys. **13**, 829 (2017).
[64] A V Chumak and H Schultheiss, Magnonics: Spin waves connecting charges, spins and photons, J. Phys. D **50**, 300201 (2017).
[65] Matthias Althammer, Pure spin currents in magnetically ordered insulator/normal metal heterostructures, J. Phys. D **51**, 313001 (2018).
[66] L. J. Cornelissen, J. Liu, R. A. Duine, J. Ben Youssef, and B. J. van Wees, Long-distance transport of magnon spin information in a magnetic insulator at room temperature, Nat. Phys. **11**, 1022 (2015).
[67] Sebastian T. B. Goennenwein, Richard Schlitz, Matthias Pernpeintner, Kathrin Ganzhorn, Matthias Althammer, Rudolf Gross, and Hans Huebl, Non-local magnetoresistance in YIG/Pt nanostructures, Appl. Phys. Lett. **107**, 172405 (2015).
[68] V. E. Demidov, S. Urazhdin, B. Divinskiy, V. D. Bessonov, A. B. Rinkevich, V. V. Ustinov, and S. O. Demokritov, Chemical potential of quasi-equilibrium magnon gas driven by pure spin current, Nat. Commun. **8**, 1579 (2017).
[69] Kevin S. Olsson, Kyongmo An, Gregory A. Fiete, Jianshi Zhou, Li Shi, and Xiaoqin Li, Pure spin current and magnon chemical potential in a nonequilibrium magnetic insulator, Phys. Rev. X **10**, 021029 (2020).
[70] Richard Schlitz, Saül Vélez, Akashdeep Kamra, Charles-Henri Lambert, Michaela Lammel, Sebastian T. B. Goennenwein, and Pietro Gambardella, Control of nonlocal magnon spin transport via magnon drift currents, Phys. Rev. Lett. **126**, 257201 (2021).
[71] T. Holstein and H. Primakoff, Field dependence of the intrinsic domain magnetization of a ferromagnet, Phys. Rev. **58**, 1098 (1940).
[72] L. D. Landau, E. M. Lifšic, E. M. Lifshitz, A. M. Kosevich, J. B. Sykes, L. P. Pitaevskii, and W. H. Reid, *Theory of Elasticity: Volume 7*, Course of Theoretical Physics (Elsevier Science, Amsterdam, 1986).
[73] N. Levy, S. A. Burke, K. L. Meaker, M. Panlasigui, A. Zettl, F. Guinea, A. H. Castro Neto, and M. F. Crommie, Strain-induced pseudo-magnetic fields greater than 300 Tesla in graphene nanobubbles, Science **329**, 544 (2010).
[74] M. A. H. Vozmediano, M. I. Katsnelson, and F. Guinea, Gauge fields in graphene, Phys. Rep. **496**, 109 (2010).
[75] Fernando de Juan, Juan L. Mañes, and María A. H. Vozmediano, Gauge fields from strain in graphene, Phys. Rev. B **87**, 165131 (2013).
[76] Gerardo G Naumis, Salvador Barraza-Lopez, Maurice Oliva-Leyva, and Humberto Terrones, Electronic and optical properties of strained graphene and other strained 2D materials: A review, Rep. Prog. Phys. **80**, 096501 (2017).
[77] Dawei Zhai and Nancy Sandler, Electron dynamics in strained graphene, Mod. Phys. Lett. B **33**, 1930001 (2019).
[78] Si-Yu Li, Ying Su, Ya-Ning Ren, and Lin He, Valley polarization and inversion in strained graphene via pseudo-Landau levels, valley splitting of real Landau levels, and confined states, Phys. Rev. Lett. **124**, 106802 (2020).
[79] Geremia Massarelli, Gideon Wachtel, John Y. T. Wei, and Arun Paramekanti, Pseudo-Landau levels of Bogoliubov quasiparticles in strained nodal superconductors, Phys. Rev. B **96**, 224516 (2017).
[80] Emilian M. Nica and Marcel Franz, Landau levels from neutral Bogoliubov particles in two-dimensional nodal superconductors under strain and doping gradients, Phys. Rev. B **97**, 024520 (2018).
[81] Stephan Rachel, Lars Fritz, and Matthias Vojta, Landau levels of Majorana fermions in a spin liquid, Phys. Rev. Lett. **116**, 167201 (2016).
[82] Ran Cheng, Satoshi Okamoto, and Di Xiao, Spin Nernst effect of magnons in collinear antiferromagnets, Phys. Rev. Lett. **117**, 217202 (2016).
[83] Vladimir A. Zyuzin and Alexey A. Kovalev, Magnon spin Nernst effect in antiferromagnets, Phys. Rev. Lett. **117**, 217203 (2016).
[84] Y. Shiomi, R. Takashima, and E. Saitoh, Experimental evidence consistent with a magnon Nernst effect in the antiferromagnetic insulator $MnPS_3$, Phys. Rev. B **96**, 134425 (2017).
[85] Rina Takashima, Yuki Shiomi, and Yukitoshi Motome, Nonreciprocal spin Seebeck effect in antiferromagnets, Phys. Rev. B **98**, 020401(R) (2018).

[86] Hiroki Kondo and Yutaka Akagi, Nonlinear magnon spin Nernst effect in antiferromagnets and strain-tunable pure spin current, Phys. Rev. Res. **4**, 013186 (2022).
[87] F. Feringa, J. M. Vink, and B. J. van Wees, Spin Nernst magnetoresistance for magnetization study of $FePS_3$, Phys. Rev. B **107**, 094428 (2023).
[88] Di Xiao, Ming-Che Chang, and Qian Niu, Berry phase effects on electronic properties, Rev. Mod. Phys. **82**, 1959 (2010).
[89] Felix von Oppen, Francisco Guinea, and Eros Mariani, Synthetic electric fields and phonon damping in carbon nanotubes and graphene, Phys. Rev. B **80**, 075420 (2009).
[90] V. Miseikis, J. E. Cunningham, K. Saeed, R. O'Rorke, and A. G. Davies, Acoustically induced current flow in graphene, Appl. Phys. Lett. **100**, 133105 (2012).
[91] Abolhassan Vaezi, Nima Abedpour, Reza Asgari, Alberto Cortijo, and María A. H. Vozmediano, Topological electric current from time-dependent elastic deformations in graphene, Phys. Rev. B **88**, 125406 (2013).
[92] A. V. Kalameitsev, V. M. Kovalev, and I. G. Savenko, Valley acoustoelectric effect, Phys. Rev. Lett. **122**, 256801 (2019).
[93] K. Sonowal, A. V. Kalameitsev, V. M. Kovalev, and I. G. Savenko, Acoustoelectric effect in two-dimensional Dirac materials exposed to Rayleigh surface acoustic waves, Phys. Rev. B **102**, 235405 (2020).
[94] P. O. Sukhachov and H. Rostami, Acoustogalvanic effect in Dirac and Weyl semimetals, Phys. Rev. Lett. **124**, 126602 (2020).
[95] Eran Sela, Yakov Bloch, Felix von Oppen, and Moshe Ben Shalom, Quantum Hall response to time-dependent strain gradients in graphene, Phys. Rev. Lett. **124**, 026602 (2020).
[96] Pankaj Bhalla, Giovanni Vignale, and Habib Rostami, Pseudogauge field driven acoustoelectric current in two-dimensional hexagonal Dirac materials, Phys. Rev. B **105**, 125407 (2022).
[97] Pai Zhao, Chithra H. Sharma, Renrong Liang, Christian Glasenapp, Lev Mourokh, Vadim M. Kovalev, Patrick Huber, Marta Prada, Lars Tiemann, and Robert H. Blick, Acoustically induced giant synthetic Hall voltages in graphene, Phys. Rev. Lett. **128**, 256601 (2022).
[98] Yuya Ominato, Daigo Oue, and Mamoru Matsuo, Valley transport driven by dynamic lattice distortion, Phys. Rev. B **105**, 195409 (2022).
[99] Sergio M. Rezende, Antonio Azevedo, and Roberto L. Rodríguez-Suárez, Introduction to antiferromagnetic magnons, J. Appl. Phys. **126**, 151101 (2019).
[100] Our strategy provides an intrinsic magnon spin Hall effect even in topologically trivial antiferromagnets: $\int [d\boldsymbol{k}] \boldsymbol{\Omega}^{\alpha(\beta)} = 0$. This fact is quite different from the previous studies on the magnon thermal Hall effect, which relies on topologically nontrivial magnon bands. Furthermore, the thermal Hall current vanishes in the absence of the Dzyaloshinskii-Moriya interaction, and hence the only remaining net current is the spin Hall current. For detailed calculations, see the Supplemental Material [57].
[101] Wenyu Xing, Luyi Qiu, Xirui Wang, Yunyan Yao, Yang Ma, Ranran Cai, Shuang Jia, X. C. Xie, and Wei Han, Magnon transport in quasi-two-dimensional Van der Waals antiferromagnets, Phys. Rev. X **9**, 011026 (2019).
[102] D. Kobayashi, T. Yoshikawa, M. Matsuo, R. Iguchi, S. Maekawa, E. Saitoh, and Y. Nozaki, Spin current generation using a surface acoustic wave generated via spin-rotation coupling, Phys. Rev. Lett. **119**, 077202 (2017).
[103] Shoma Tateno, Genki Okano, Mamoru Matsuo, and Yukio Nozaki, Electrical evaluation of the alternating spin current generated via spin-vorticity coupling, Phys. Rev. B **102**, 104406 (2020).
[104] A. R. Wildes, S. Okamoto, and D. Xiao, Search for nonreciprocal magnons in $MnPS_3$, Phys. Rev. B **103**, 024424 (2021).
[105] Even Thingstad, Akashdeep Kamra, Arne Brataas, and Asle Sudbø, Chiral phonon transport induced by topological magnons, Phys. Rev. Lett. **122**, 107201 (2019).
[106] Gyungchoon Go, Se Kwon Kim, and Kyung-Jin Lee, Topological magnon-phonon hybrid excitations in two-dimensional ferromagnets with tunable Chern numbers, Phys. Rev. Lett. **123**, 237207 (2019).
[107] Sungjoon Park, Naoto Nagaosa, and Bohm-Jung Yang, Thermal Hall effect, spin Nernst effect, and spin density induced by a thermal gradient in collinear ferrimagnets from magnon-phonon interaction, Nano Lett. **20**, 2741 (2020).
[108] Shu Zhang, Gyungchoon Go, Kyung-Jin Lee, and Se Kwon Kim, Su(3) topology of magnon-phonon hybridization in 2D antiferromagnets, Phys. Rev. Lett. **124**, 147204 (2020).
[109] N. Bazazzadeh, M. Hamdi, S. Park, A. Khavasi, S. M. Mohseni, and A. Sadeghi, Magnetoelastic coupling enabled tunability of magnon spin current generation in two-dimensional antiferromagnets, Phys. Rev. B **104**, L180402 (2021).
[110] S. A. Owerre, Magnonic analogs of topological Dirac semimetals, J. Phys. Commun. **1**, 025007 (2017).
[111] The electronic spin Hall effect is prohibited under the time-reversal symmetry as can be seen in Table I. Therefore, the emergence of a net spin Hall current by pseudoelectric fields is unique to the magnonic systems.